Modeling and Inverse Compensation of Nonmonotonic Hysteresis in VO_2-Coated Microactuators

Jun Zhang, *Student Member, IEEE*, Emmanuelle Merced, Nelson Sepúlveda, *Senior Member, IEEE*, and Xiaobo Tan, *Senior Member, IEEE*

***Abstract*—Vanadium dioxide (VO_2) undergoes a thermally induced solid-to-solid phase transition, which can be exploited for actuation purposes. VO_2-coated silicon cantilevers demonstrate abrupt curvature changes when their temperature is varied across the phase transition. Unlike the monotonic hysteresis phenomena observed in many other smart materials, the curvature–temperature hysteresis of VO_2 actuators is nonmonotonic due to competing mechanisms associated with the material's phase transition and the different thermal expansion coefficients of the materials that form the bilayered cantilever. Motivated by the underlying physics, a novel model for the nonmonotonic hysteresis that combines a monotonic Preisach hysteresis operator and a quadratic operator is presented. A constrained least-squares scheme is proposed for model identification, and an effective inverse control scheme is presented for hysteresis compensation. For comparison purposes, a Preisach operator with a signed density function and a single-valued polynomial model are considered. Experimental results show that, for a 300-μm-long actuator, the largest modeling errors with the proposed model, the signed Preisach operator, and the polynomial approximation are 46.8, 80.3, and 483 m^{-1}, respectively, over the actuated curvature range of $[-104,\ 1846]\ \mathrm{m}^{-1}$. In addition, both the largest tracking error and root-mean-square error under the proposed inversion scheme are only around 10% of those under the polynomial-based inversion scheme.**

***Index Terms*—Inverse compensation, nonmonotonic hysteresis, phase-transition materials, Preisach operator, vanadium dioxide (VO_2).**

I. Introduction

VANADIUM dioxide (VO_2) is a novel smart material that undergoes a thermally induced solid-to-solid phase transition around 68 °C [1]. During the transition, the material's crystalline structure changes from a monoclinic phase (M_1) at low temperatures to a tetragonal phase (R) at high temperatures, which results in drastic changes in the electrical, mechanical, electromagnetic, and optical properties of the material. These characteristics make VO_2 a promising multifunctional material for sensors [2], actuators [3]–[5], and memory applications [6]. The actuation potential of VO_2 was not noticed until recently [3]. By coating VO_2 on a microstructure (e.g., a silicon cantilever), thermally actuated microbenders can be created, which have shown full reversible actuation, large bending, and high energy density [5], making them particularly suitable for applications such as micromanipulation and microrobotics.

The realization of the potential of VO_2-coated microactuators, however, is greatly hindered by their sophisticated nonmonotonic hysteretic behavior resulting from two competing actuation effects. The first actuation effect is due to the internal stress generated during the phase transition, which is inherently hysteretic with respect to temperature. The second actuation effect is due to the differential thermal expansion of the VO_2 layer and the substrate, which causes an opposite bending effect. While the thermal expansion effect persists throughout the temperature range, the stress generated during the VO_2's structural changes dominates across the phase transition [4]. As a result, the relationship between the bending curvature and temperature is *nonmonotonic* when the temperature is raised or lowered monotonically. This nonmonotonic hysteresis presents challenges in the modeling and control of VO_2 microactuators.

Modeling and control of systems with hysteresis has been an active research area, especially in the field of smart materials-based systems [7]–[15]. A very popular phenomenological hysteresis model is the Preisach operator, which has proven effective in capturing complex, hysteretic behavior in various smart materials, such as piezoelectrics [7], shape memory alloys [14], and magnetostrictives [15]. The wide spread of smart material-actuated systems has also spurred the development of control schemes for systems with hysteresis. A predominant class of hysteresis control approaches involves approximate cancellation of the hysteresis effect through inversion [7], [10]–[12], [15].

Despite the aforementioned extensive work on modeling and control of hysteresis in smart materials, most studies have focused on monotonic hysteresis nonlinearities [7]–[15], where a monotonic input causes a monotonic output. A special type of nonmonotonic hysteresis with butterfly-shaped hysteresis loops was investigated by Drincic *et al.* [16]; however, the study there was focused on hysteresis loops that can be converted to monotonic hysteresis through unimodal mappings.

Manuscript received June 15, 2012; revised November 8, 2012 and January 24, 2013; accepted February 21, 2013. Date of publication March 20, 2013; date of current version February 20, 2014. Recommended by Technical Editor K. K. Leang. This work was supported in part by the National Science Foundation under Grant ECCS 0547131 and Grant CMMI 0824830. The work of E. Merced was supported by the National Science Foundation under Grant DGE-0802267 (Graduate Research Fellowship Program).

The authors are with the Department of Electrical and Computer Engineering, Michigan State University, East Lansing, MI 48824 USA (e-mail: zhangj78@egr.msu.edu; mercedem@egr.msu.edu; nelsons@egr.msu.edu; xbtan@egr.msu.edu).

Color versions of one or more of the figures in this paper are available online at http://ieeexplore.ieee.org.

Digital Object Identifier 10.1109/TMECH.2013.2250989

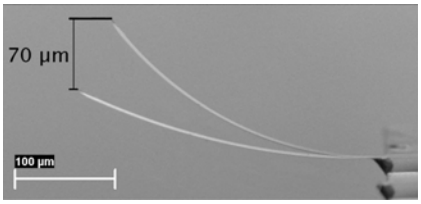

Fig. 1. Superimposed SEM pictures of the 300-μmVO_2-coated silicon cantilever taken when the substrate temperature was 30 °C (lower curvature) and 90 °C (higher curvature), respectively.

This paper presents, to the authors' best knowledge, the *first* systematic studies on the modeling and inverse compensation of nonmonotonic hysteresis exhibited by VO_2-coated microactuators. First, a physics-motivated model that accounts for the two (opposite) actuation mechanisms is presented. The first mechanism is the stress resulting from structural changes in VO_2, which is modeled with a monotonic Preisach operator. The second mechanism is the differential thermal expansion. Since the thermal expansion coefficient (TEC) of VO_2 depends on the phase mixture of the material, a linear function of the temperature is taken to efficiently model the phase fraction of VO_2, which results in a quadratic operator for the thermal expansion-induced actuation. The parameters of the model are identified. Second, an efficient inverse compensation scheme is developed for the proposed nonmonotonic hysteresis model by adapting the scheme used in [15] for a Preisach operator with nonnegative, piecewise constant density function. The effectiveness of the model and the inverse compensation scheme is demonstrated in experiments, with comparison to two other approaches, one based on a Preisach operator with a signed density function and the other based on a polynomial model.

II. Experimental Characterization of VO_2-Coated Microactuators

A. Material Preparation and Experimental Setup

A 172-nm-thick VO_2 layer was deposited by pulsed laser deposition on a 300-μm-long silicon cantilever (MikroMasch CSC12) with width and thickness of 35 and 1 μm, respectively. The deposition was conducted inside a vacuum chamber. The deposition followed a similar procedure as in previous experiments [3], where a krypton fluoride excimer laser (Lambda Physik LPX 200, $\lambda = 248$ nm) was focused on a rotating metallic vanadium target with a 10 Hz repetition rate. The background pressure was 10^{-6} Torr and throughout the deposition was kept at 20 mTorr with gas flows of 10 (argon) and 15 (oxygen) standard cubic centimeter per minute.

Fig. 1 shows two superimposed scanning electron microscopy (SEM) pictures of the prepared VO_2-coated cantilever, when the substrate temperature was 30 and 90 °C, respectively. VO_2 is in pure M_1 and R phases at those two temperatures. A total tip displacement change of about 70 μm is observed in Fig. 1, illustrating the large bending the microactuator is capable of generating. The considerable amount of initial curvature at room temperature is due to the residual stress after deposition. Since the change of curvature is of more interest, the curvature change from the initial curvature is taken as the output in this paper.

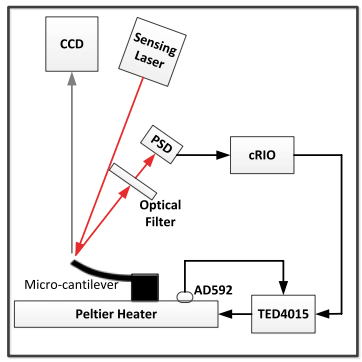

Fig. 2. Setup used for measuring the cantilever tip deflection as a function of temperature.

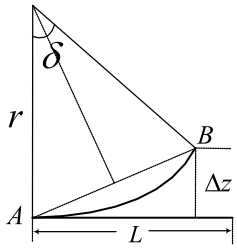

Fig. 3. Illustration of the geometric relationship between the curvature and the tip deflection of a bent cantilever.

In order to experimentally measure the tip deflection as a function of temperature, the setup shown in Fig. 2 was used, which was similar to the one used before [3]. Here, the microcantilever was glued with a highly thermal conductive silver paint to a glass substrate that was directly in contact with a Peltier heater. The heater was controlled in closed loop with a commercially available benchtop temperature controller (Thorlabs, TED-4015) connected to a temperature sensor (AD592), with a precision in temperature control of ± 0.1°C. A custom-made current controller circuit was used to power an infrared laser ($\lambda = 808$ nm) with a maximum power of 20 mW. The laser spot was focused on the tip of the cantilever and the reflected laser light was captured by a 1-D position sensitive detector (PSD) (Hamamatsu S3270). The PSD outputs a voltage proportional to the position of the reflected laser spot on its active area. Bending of the VO_2-coated cantilever produces an angular displacement on the reflected laser spot, which changes the output voltage of the PSD. The laser intensity was kept at the lowest detectable by the PSD, in order to obtain good signal-to-noise ratio, while minimizing heating of the cantilever by the laser. The output voltage from the PSD was measured with an analog input module (NI 9201), which was attached to an embedded real-time controller (NI cRIO 9075), and a LabView program was created in order to automate the deflection measurements.

The measured tip deflection Δz was converted to the curvature κ using the geometry illustrated in Fig. 3. The radius of

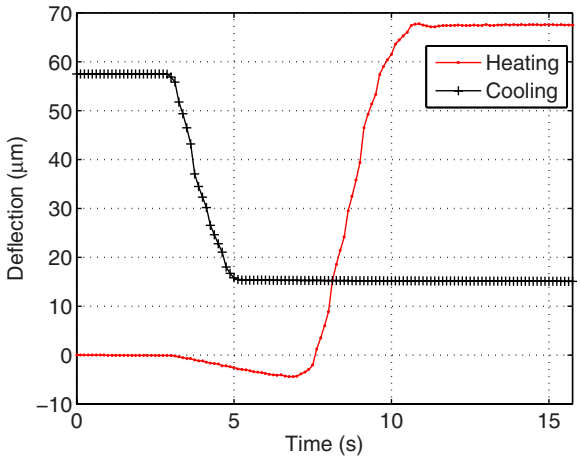

Fig. 4. Deflection as a function of time through heating and cooling temperature steps. There is no observable creep.

curvature, $r = 1/\kappa$, is related to Δz via

$$\Delta z = \sin\left(\frac{\delta}{2}\right) \cdot AB = 2r \cdot \sin^2\left(\frac{L}{2r}\right) \tag{1}$$

where $\delta = \frac{L}{r}$. For the microactuator studied in this paper, the small-angle approximation typically used ($\Delta z \approx \frac{L^2}{2r}$) will not be valid because of the large bending, and the transcendental equation (1) is numerically solved for the curvature.

B. Characterization of Nonmonotonic Hysteresis

A creep test was conducted and no obvious creep was found. The temperature was varied by a step and then until constant, while the deflection was measured for the whole process. As Fig. 4 shows, the deflection under unchanged temperature values varied from 67.378 to 67.667 μm and from 15.082 to 15.164 μm, respectively. These minute variations are mainly attributed to error in temperature control (accuracy $\pm 0.1\,^{\circ}$C); hence, creep is not considered in this paper.

A set of experiments were conducted to obtain the curvature of the VO_2 microactuator as a function of temperature. The temperature range was chosen to be from 21 to 84 °C, to fully cover the phase transition regime. The temperature profile in time followed a pattern of damped oscillations (not shown), to provide sufficiently rich excitation for the identification of the Preisach hysteresis model [17]. Fig. 5(a) shows the measured nested hysteresis loops between the actuator curvature and temperature. Notice that the apparent phase transition temperature is shifted from the typical value of 68 °C. This is attributed to the heating effect by the deflection-measuring laser; recall that the recorded temperature was only for the Peltier heater located underneath the sample. In this paper, the heat contribution from the measurement laser is considered to be constant (which is a reasonable assumption), and thus, the temperature of the Peltier heater is taken as the input.

Nonmonotonic hysteresis can be clearly observed in Fig. 5(a). As the temperature is increased, the curvature first decreases slightly, then increases abruptly, and finally decreases slightly again when the temperature is sufficiently high. An analogous

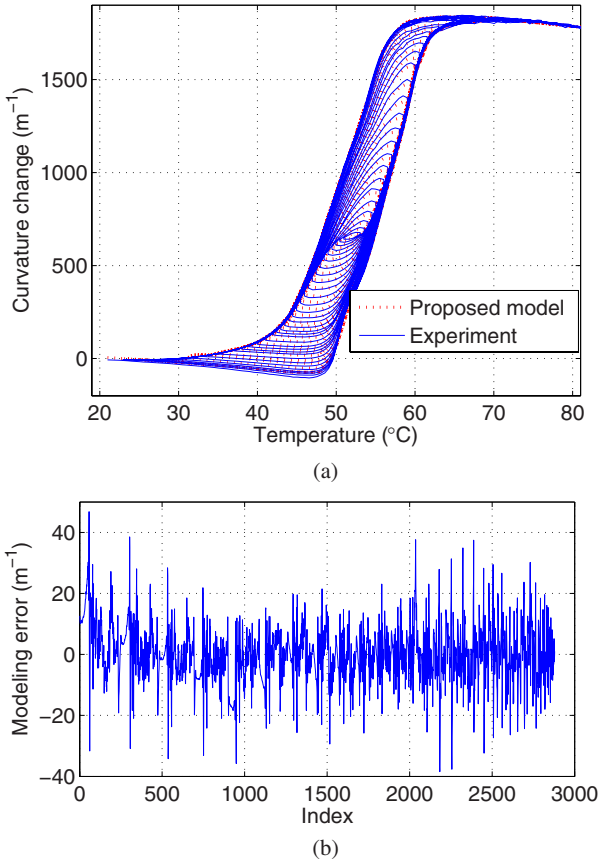

Fig. 5. Proposed model. (a) Measured nonmonotonic curvature–temperature hysteresis and that based on the proposed model. (b) Modeling error for the entire temperature sequence.

trend holds true when the temperature is decreased. The nonmonotonic behavior can be explained by two competing actuation mechanisms. On one hand, changes in the crystalline structures during the $M_1 \rightarrow R$ phase transition result in microcantilever bending toward the VO_2 layer. Vanadium ions are reordered during the phase transition, where one unit cell in the M_1 phase corresponds to two unit cells in the R phase. The crystalline plane parallel to the substrate changes from $(011)_{M_1}$ in the M_1 phase to $(110)_R$ in the R phase. From the lattice parameters [18], it is calculated that the crystallographic plane of VO_2 that is parallel to the cantilever surface for this case ($(011)_M$) decreases its area by 1.7% (on heating), which generates a strain of approximately -0.083 [3], causing a drastic bending toward the VO_2 layer side. On the other hand, since the TEC of VO_2 for both the M_1 phase and the R phase [18] are larger than that of silicon [19], the differential thermal expansion-induced stresses result in an opposite bending effect from that of the phase transition effect.

There are several additional interesting observations from Fig. 5(a). First, the curvature–temperature relationship is hysteretic only in the intermediate temperature regime and becomes a single-valued function at both the low- and high-temperature ends. This provides support for the two actuation effects discussed earlier; phase transition dominates the intermediate temperature region, while at the low- or high-temperature ends, VO_2

is in a single phase (M_1 or R phase, respectively), and the differential thermal expansion takes dominance. Second, the slope of curvature versus temperature at the low-temperature end is different from that at the high-temperature end, suggesting that the TEC of VO_2 changes with the material phase. This is consistent with what can be found in the literature [18].

We have also conducted extensive experiments to characterize the repeatability of the actuation behavior and found that hysteresis loops measured on different days (with the same temperature input sequence) are nearly identical. Details of these results are not included here in the interest of brevity.

III. Modeling of the Nonmonotonic Hysteresis

A. Actuation Effect due to Phase Transition

The proposed model for the curvature output κ of the VO_2-coated cantilever comprises the contribution κ_P due to the phase transition and the contribution κ_E due to the differential thermal expansion. The phase transition contribution is monotonically hysteretic with respect to the temperature T, thus will be modeled by a Preisach operator [20], [21] with nonnegative density function μ

$$\begin{aligned}\kappa_P(t) &= \Gamma[T(\cdot);\zeta_0](t)\\ &= c_0 + \int_{\mathcal{P}_0} \mu(\beta,\alpha)\gamma_{\beta,\alpha}[T(\cdot);\zeta_0(\beta,\alpha)](t)d\beta\, d\alpha. \quad (2)\end{aligned}$$

Here, c_0 is some constant bias, $T(\cdot)$ denotes the temperature history, $T(\tau)$, $0 \le \tau \le t$, $\mathcal{P}_0$ is called the Preisach plane $\mathcal{P}_0 \triangleq \{(\beta,\alpha) : T_{\min} \le \beta \le \alpha \le T_{\max}\}$, where $[T_{\min}, T_{\max}]$ denotes the temperature range for phase transition, and finally, $\gamma_{\beta,\alpha}$ denotes the basic hysteretic unit (hysteron): for a pair of thresholds (β,α) and an initial condition $\zeta_0(\beta,\alpha) \in \{-1,1\}$, the output of the hysteron is defined as

$$u(t) = \gamma_{\beta,\alpha}[T(\cdot);\zeta_0(\beta,\alpha)] = \begin{cases} +1, & \text{if } T(t) > \alpha \\ -1, & \text{if } T(t) < \beta \\ u(t^-), & \text{if } \beta \le T(t) \le \alpha \end{cases} \quad (3)$$

where $T(\cdot)$ is the temperature input history $T(\tau), 0 \le \tau \le t$, and $u(t^-) = \lim_{\epsilon>0,\epsilon\to 0} u(t-\epsilon)$.

Note that $\mathcal{P}_0$ can be divided into two regions according to the outputs of hysterons, and the boundary of the two regions (called memory curve and denoted ψ) represents equivalently the state and thus determines the output of the Preisach operator. For this reason, the initial state function ζ_0 can be replaced by an initial memory curve in the Preisach plane.

B. Differential Thermal Expansion Effect

When the temperature increases (decreases, respectively), a material typically expands (shrinks, respectively). For a two-layer beam, the difference in the thermal expansion of individual layers results in bending. The VO_2-coated silicon cantilever curvature κ_E due to differential thermal expansion at a temperature T can be derived following standard analysis [22]:

$$\kappa_E = -\frac{6(1+m)^2(C_{VO_2} - C_{Si})(T - T_0)}{h\left(3(1+m)^2 + (1+mw)(m^2 + \frac{1}{mw})\right)} \quad (4)$$

where h is the total thickness of the beam, m is the ratio of the VO_2 layer thickness to that of the silicon layer, w is the ratio of the modulus of elasticity of the VO_2 layer to that of the silicon layer, C_{VO_2} and C_{Si} are the TECs of the VO_2 and silicon, respectively, and T_0 is the room temperature (20 °C). In (4), it is defined that κ_E is positive when the beam bends toward the VO_2 layer.

As mentioned earlier, the TEC of VO_2 in the M_1 phase is different from that in the R phase. Since the phase transition spans through the temperature range $[T_{\min}, T_{\max}]$, both phases coexist within that temperature range. If C_{M_1} and C_R are the TECs of VO_2 in the M_1 and R phases, respectively, and $\theta(T)$ is the material fraction of the R phase at a particular temperature T, then the effective TEC of VO_2 during the phase transition can be represented with respect to T as

$$C_{VO_2} = (1-\theta(T))C_{M_1} + \theta(T)C_R. \quad (5)$$

In general, the R phase fraction θ is hysteretic with respect to the temperature T. To make the problem tractable, θ is approximated by a linear function of T, which is supported by experimental observations [23]

$$\theta = \begin{cases} 0, & \text{if } T < T_{\min} \\ \dfrac{T - T_{\min}}{T_{\max} - T_{\min}}, & \text{if } T_{\min} \le T \le T_{\max} \\ 1, & \text{if } T > T_{\max}. \end{cases} \quad (6)$$

Combining (4) and (5), we rewrite κ_E as

$$\kappa_E = -\left(k_0(1-\theta(T)) + k_1\theta(T)\right)(T - T_0) \quad (7)$$

where $k_0 = \frac{6(1+m)^2(C_{M_1} - C_{Si})}{h\left(3(1+m)^2 + (1+mw)(m^2+\frac{1}{mw})\right)}$ and $k_1 = \frac{6(1+m)^2(C_R - C_{Si})}{h\left(3(1+m)^2 + (1+mw)(m^2+\frac{1}{mw})\right)}$. Since $C_{M_1} < C_R$ [18], $k_1 > k_0$. With the approximation (6) for $\theta(T)$, the differential thermal expansion-induced curvature has a quadratic dependence on T.

By adding (2) and (7), we obtain the total curvature with a new hysteresis operator Ω

$$\begin{aligned}\kappa(t) &= \kappa_P(t) + \kappa_E(t) = \Omega[T(\cdot);\zeta_0](t)\\ &\triangleq c_0 + \Gamma[T(\cdot);\zeta_0](t) - \left(k_0(1-\theta(T(t)))\right)(T(t) - T_0)\\ &\quad + k_1\theta(T(t))(T(t) - T_0). \quad (8)\end{aligned}$$

Note that for Ω, only the contribution κ_P is memory-dependent, so Ω shares the same state (or memory curve) as Γ. In particular, they will share the same initial memory curve.

IV. Model Identification and Validation

A. Parameter Identification

The parameters of the model (8) include the density function μ of the Preisach operator, and the constants c_0, k_0, and k_1. For the identification of a Preisach density function, a discretization step is typically involved. The discretization scheme adopted in this paper approximates the density by a piecewise constant function, where the density value is constant within each lattice cell but varies from cell to cell [24].

The input range is discretized uniformly into M levels, which results in $M(M+1)/2$ cells, leading to a total of $K = M(M+1)/2$ weight parameters. The actual operating range for the input, $[T'_{\min}, T'_{\max}]$, is considered larger than the phase transition region $[T_{\min}, T_{\max}]$. In other words, $T'_{\min} < T_{\min} < T_{\max} < T'_{\max}$.

In a discrete time setting, the contribution $\kappa_P[n]$ at time n is

$$\kappa_P[n] = c_0 + \sum_{i=1}^{M} \sum_{j=1}^{M+1-i} \mu_{ij} s_{ij}[n] \tag{9}$$

where $s_{ij}[n]$ represents the *signed* area of cell (i, j), and μ_{ij} represents the density of cell (i, j). Note that the signed area of each cell is defined as the area occupied by hysterons with output $+1$ minus that occupied by hysterons with output -1. For ease of presentation, the cells (i, j) are ordered with a single index $l = 1, 2, \ldots, K$, and the density and signed area of the lth cell are denoted (with abuse of notation) by μ_l and s_l, respectively. Equation (9) is rewritten as

$$\kappa_P[n] = c_0 + \sum_{l=1}^{K} \mu_l s_l[n]. \tag{10}$$

When the input $T[n]$ is in $[T'_{\min}, T_{\min}]$, all hysterons attain the value of -1 and the Preisach operator is at the negative saturation, $\kappa_P[n] = c_0 - \kappa_0$, where $\kappa_0 = \sum_{l=1}^{K} \mu_l$. Similarly, positive saturation is reached when the temperature $T[n]$ is within $[T_{\max}, T'_{\max}]$.

On the other hand, the contribution $\kappa_E[n]$ is

$$\kappa_E[n] = -\left(k_0(1 - \theta(T[n])) + k_1\theta(T[n])\right)(T[n] - T_0). \tag{11}$$

Combining (10) and (11), we obtain the total curvature output as

$$\kappa[n] = c_0 + \sum_{l=1}^{K} \mu_l s_l[n] - \left(k_0(1 - \theta(T[n])) + k_1\theta(T[n])\right)(T[n] - T_0). \tag{12}$$

Preisach density functions are assumed to be nonnegative, $\mu_l \geq 0$. In addition, k_0 and k_1 are positive from their physical meanings. Finally, $c_0 > 0$ since VO_2-coated microcantilevers have positive curvature bias. A constrained least-squares method, realized with the MATLAB command *lsqnonneg*, is utilized to identify the vector of parameters, $[\mu_1 \ \ \mu_2 \ \ \mu_3 \ \cdots \ \ \mu_K \ \ c_0 \ \ k_0 \ \ k_1]^T$, that meets the sign constraints.

B. Experimental Results

To effectively identify the model parameters, the input needs to provide sufficient excitation for all cells of the Preisach operator. One type of such input sequences takes the form of damped oscillations, which produces nested hysteresis loops [17] and is adopted in this paper. Based on empirical knowledge, the temperature of the closed-loop-controlled Peltier device can settle around a set temperature within about 3 s. A wait time of 8 s was chosen between temperature setpoints to ensure that the thermal steady state has been reached. While the experiment will remain to be quasi-static if the waiting time is longer than 8 s, it is not advisable to make it much shorter.

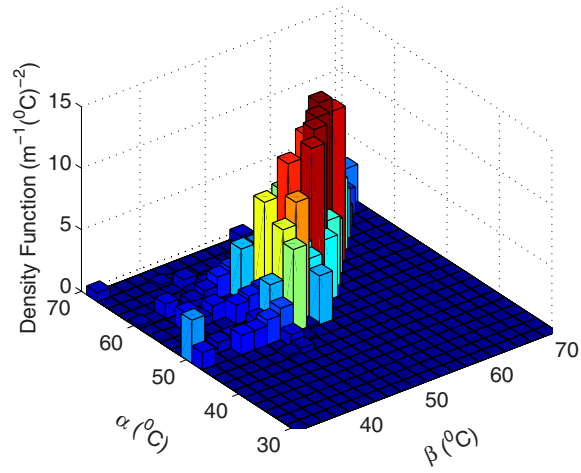

Fig. 6. Identified Preisach density function for the proposed model.

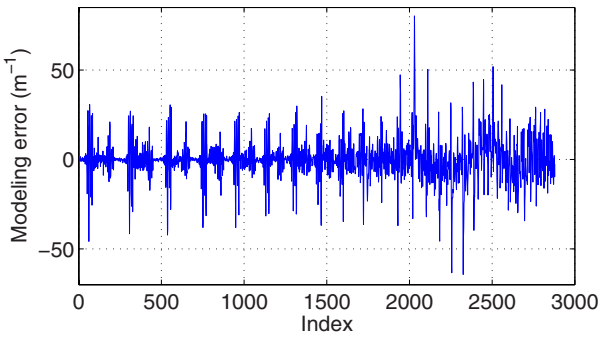

Fig. 7. Modeling error with the signed Preisach operator for the entire temperature sequence.

The full range of temperature input $[T'_{\min}, T'_{\max}]$ is $[21, 84]^\circ$C. From Fig. 5(a), the phase transition region $[T_{\min}, T_{\max}]$ is determined to be $[30, 70]^\circ$C. The level of discretization M for the Preisach plane is chosen to be 20. Fig. 5(a) compares the measured hysteresis loops and those based on the identified model, and Fig. 5(b) shows the corresponding modeling error for the entire temperature sequence, which is mostly bounded by 30 m^{-1}, compared with the total curvature change range $[-104, \ 1846]$ m^{-1}. Fig. 6 shows the identified density function of the Preisach operator. c_0, k_0, and k_1 have been identified to be 1026.7 m^{-1}, 2.8 $\mathrm{m}^{-1} \cdot \mathrm{K}^{-1}$, and 4.3 $\mathrm{m}^{-1} \cdot \mathrm{K}^{-1}$, respectively.

For comparison purposes, two additional models for the nonmonotonic hysteresis are considered: a Preisach operator with a signed density function, and a nonlinear single-valued function represented by a high-degree polynomial.

The signed Preisach operator is identified with a similar procedure as in Section IV-A, where there are no sign constraints placed on the Preisach densities. The level of discretization M for the Preisach plane is also chosen to be 20, but now is for the entire input range $[T'_{\min}, T'_{\max}] = [21, 84]^\circ$C. Fig. 7 shows the modeling error, which is larger than the proposed model. It is interesting to notice that the negative density values of the

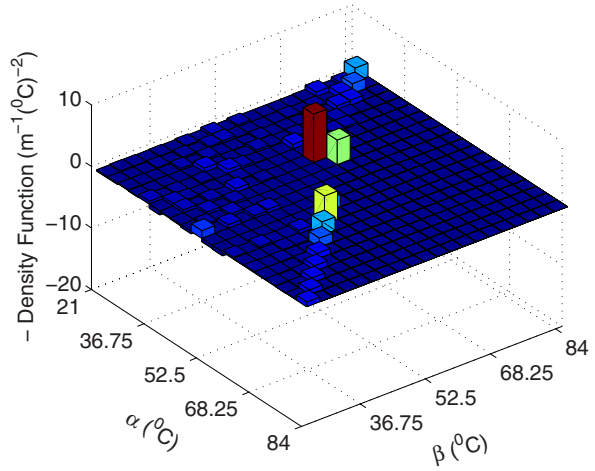

Fig. 8. Negative of the identified density values for the signed Preisach operator. The negative is taken here so that the negative elements of the density function can be seen (on top); the positive elements are now flipped to the bottom of the plane, which are not visible here.

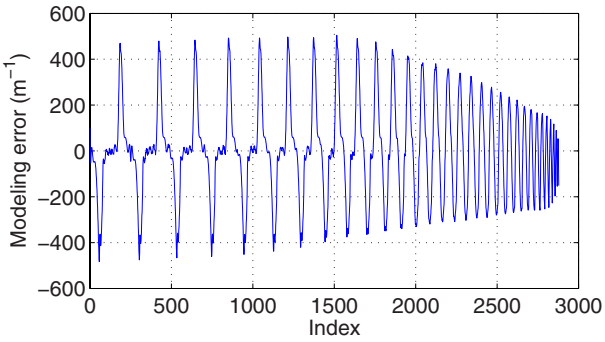

Fig. 9. Modeling error with a polynomial model for the entire temperature sequence.

signed Preisach operator are primarily located at the $\beta = \alpha$ line (see Fig. 8). This provides support for the proposed model; after all, the nonhysteretic, negative component in the proposed model that accounts for differential thermal expansion could be represented as negative densities located on the $\alpha = \beta$ line.

For the single-valued nonlinear approximation, a polynomial of degree 12 is chosen, the coefficients of which are found through a polynomial fitting between curvature measurements and the model predictions. It is not surprising that this model results in the largest modeling error among the three models explored, which is around 500 m^{-1} (see Fig. 9). This model fails to account for the hysteresis effect.

In order to further validate the proposed model, the VO_2 actuator is subjected to a randomly chosen temperature sequence, shown in Fig. 10(a), and the output curvature data (not shown) are then collected. Fig. 10(b) shows the model prediction errors. The maximum prediction errors are 108.1, 108.8, and 478.1 m^{-1} for the proposed model, the signed Preisach operator, and the polynomial model, respectively. It is clear that, with an error of less than 5.6% over the curvature range of 1950 m^{-1}, the proposed model is effective in capturing the complex hysteretic behavior of the VO_2 actuator. While the signed Preisach operator is able to provide a modeling accuracy comparable with the

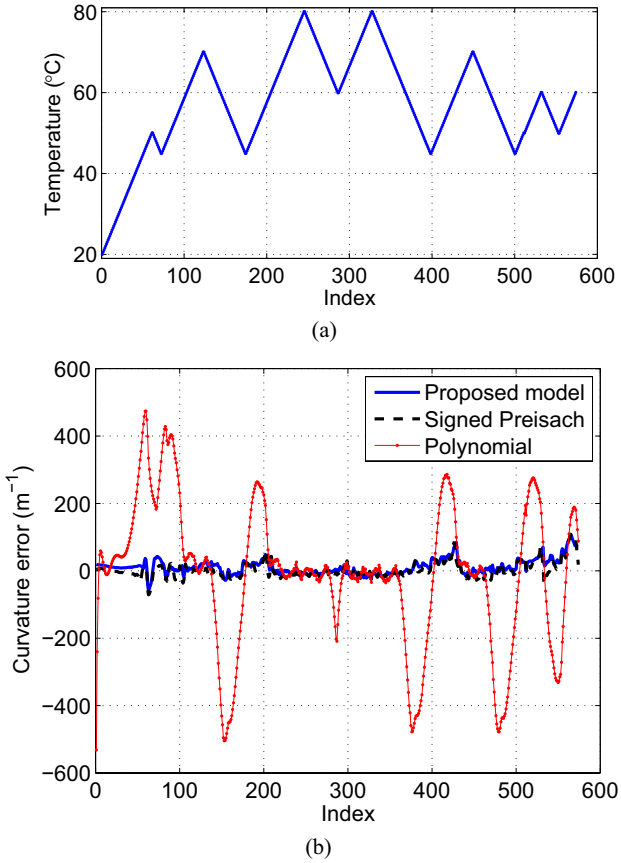

Fig. 10. (a) Randomly chosen temperature input sequence for model validation. (b) Errors in predictions by different models under the input sequence.

proposed model, it is not amenable to efficient inversion and will not be pursued further.

V. Inverse Compensation

There have been a number of inversion-related approaches for hysteresis compensation reported in the literature. For example, the direct inverse Preisach modeling method [25] aims to identify a Preisach model as the inverse operator based on empirical output/input data. The empirical temperature versus curvature hysteresis loops for VO_2 actuators [with the horizontal/vertical axes in Fig. 5(a)] exhibit sharp slope changes, making it difficult to approximate by a Preisach operator even with a prohibitively fine discretization scheme. Iterative learning control [26], [27] has proven effective in compensating both hysteresis and dynamics with relatively low requirement on modeling accuracy, but it only applies to periodic references and requires sensory feedback for the learning process. While the proposed inversion algorithm is noncausal, only the next desired output and the input history are required to obtain the input.

In this paper, we propose to compensate the hysteresis effect in VO_2 by constructing a properly defined inverse of the model presented in earlier sections. The nonmonotonic nature of the proposed hysteresis model presents several challenges in the inversion problem. In the continuous-time setting, there is great difficulty in establishing the existence and/or the

uniqueness of a continuous input function given a desired continuous output function. In the discrete-time setting, which is the case of practical interest, the concept of time-continuity is no longer relevant, since the desired output function is given as a sequence of values for the operator to achieve, and input interpolation between the sampling times is typically used to realize a quasi-continuous output for the physical system. For a monotonic hysteresis operator, for any desired output value (within the output range) $y_d[n+1]$ at next time instant $n+1$, there always exists an input value $v[n+1]$ for $n+1$, such that, if the input varies monotonically from the current value $v[n]$ to $v[n+1]$, the output y would also change monotonically from its current value $y[n]$ to $y[n+1]$, which is equal or close to $y_d[n+1]$. This, however, is no longer true for a nonmonotonic hysteresis operator as the one considered in this paper—One may not find a single input value, monotonic interpolation to which would result in the desired output value. Therefore, a *sequence* of input values needs to be found to achieve a given desired output value; without proper constraints, the latter problem would admit infinitely many solutions. A constraint on this problem is imposed to minimize the implementation complexity and assure proper output behavior: the number of elements in the computed input sequence is minimal. Specifically, for the proposed nonmonotonic hysteresis model (8), the inversion problem is formulated as follows: given the current initial memory curve $\psi^{(0)}$ for the operator Ω, with the associated temperature input $T^{(0)}$, operator output $\kappa^{(0)} = \Omega[T^{(0)}; \psi^{(0)}]$, and a target output value $\bar{\kappa}$, find a new input sequence $\bar{T}$ with minimal number of elements, such that the final value of $\Omega[\bar{T}; \psi^{(0)}]$ is equal to $\bar{\kappa}$.

The proposed inversion algorithm is adapted from the one in [15] for the inversion of a monotonic Preisach operator with a piecewise constant density function. The algorithm in [15] exploits the monotonicity of the operator and the piecewise constant nature of the density, and finds the desired input by monotonically varying the input iteratively. Assuming that the input is being increased, with the value of the kth iteration being $T^{(k)}$ and the corresponding memory curve being $\psi^{(k)}$, another increment of $d (d \le \min\{d_1^{(k)}, d_2^{(k)}\})$ in the input would result in the following change in the output of the Preisach operator:

$$\Gamma[T^{(k)} + d; \psi^{(k)}] - \Gamma[T^{(k)}; \psi^{(k)}] = a_2^{(k)} d^2 + a_1^{(k)} d \qquad (13)$$

where $d_1^{(k)} > 0$ is such that $T^{(k)} + d_1^{(k)}$ would equal the next discrete input level, and $d_2^{(k)} > 0$ is such that $T^{(k)} + d_2^{(k)}$ would erase the next corner of the memory curve; see Fig. 11 for illustration. In (13), a_1^k and $a_2^{(k)}$ are nonnegative constants associated with $\psi^{(k)}$ and the density values.

The core idea in [15] for inverting the Preisach operator is that, if $d \le \min\{d_1^{(k)}, d_2^{(k)}\}$ can be found that solves

$$a_2^{(k)} d^2 + a_1^{(k)} d = \bar{y} - \Gamma[T^{(k)}; \psi^{(k)}] \qquad (14)$$

where $\bar{y}$ is the desired output, then the required input is obtained as $T^{(k)} + d$; otherwise, let $T^{(k+1)} = T^{(k)} + \min\{d_1^{(k)}, d_2^{(k)}\}$ and continue the iteration.

Since the curvature output κ starts to decrease (increase, respectively) when $T > T_{\max}$ ($T < T_{\min}$, respectively) because

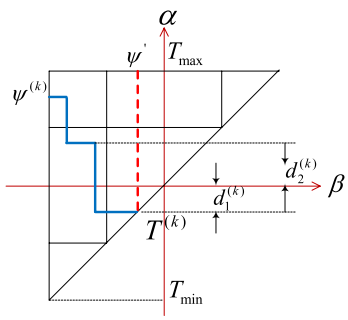

Fig. 11. Illustration of the variables $d_1^{(k)}$ and $d_2^{(k)}$ used in inversion.

κ_P becomes positively (negatively, respectively) saturated, the maximum range of curvature output can be achieved by restricting the temperature T to the range $[T_{\min}, T_{\max}]$.

From (6) and (7), the curvature contribution from differential thermal expansion is given by

$$\begin{aligned}\kappa_E = Q[T] \triangleq & \left(k_0 - \frac{(k_1 - k_0)T_{\min}}{T_{\max} - T_{\min}}\right) T_0 \\ & - T\left(k_0 - \frac{T_0 + T_{\min}}{T_{\max} - T_{\min}}(k_1 - k_0)\right) \\ & - T^2 \frac{k_1 - k_0}{T_{\max} - T_{\min}}. \end{aligned} \qquad (15)$$

Consequently, the change in κ_E for an increment d at $T^{(k)}$ is obtained as

$$Q[T^{(k)} + d] - Q[T^{(k)}] = -c_2 d^2 - c_1^{(k)} d \qquad (16)$$

where $c_1^{(k)} = k_0 - \frac{T_0 + T_{\min}}{T_{\max} - T_{\min}}(k_1 - k_0) + \frac{2(k_1 - k_0)}{T_{\max} - T_{\min}} T^{(k)}$, and $c_2 = \frac{k_1 - k_0}{T_{\max} - T_{\min}}$. Based on $T_0 \le T_{\min} \le T$ and $k_1 > k_0$ (see Section III-B), it can be shown that both $c_1^{(k)}$ and c_2 are positive.

Combining (13) and (16), we obtain

$$\begin{aligned}&\Omega[T^{(k)} + d; \psi^{(k)}] - \Omega[T^{(k)}; \psi^{(k)}] \\ &\qquad = (a_2^{(k)} - c_2) d^2 + (a_1^{(k)} - c_1^{(k)}) d. \end{aligned} \qquad (17)$$

While $a_1^{(k)} \ge 0, a_2^{(k)} \ge 0, c_1^{(k)} > 0, c_2 > 0$, the signs of both $a_1^{(k)} - c_1^{(k)}$ and $a_2^{(k)} - c_2$ could be either positive or negative, which implies that an increment d in the temperature does not necessarily lead to an increase in curvature. Analogous statements can be made when the input decreases. Take a special example of the input being increased to some value T' (with the corresponding memory curve ψ') and then decreased by a small $d > 0$, in which case $a_1^{(k)} = 0$, and $\Omega[T' - d; \psi'] - \Omega[T'; \psi'] = (a_2^{(k)} - c_2) d^2 + c_1 d$. Since the linear term dominates the quadratic term for small d, the output κ will increase immediately following the reversing of T at T'. Similarly, the curvature will decrease immediately following the reversing of a decreasing input. Interestingly, these predictions are confirmed by the experimental data, as can be seen clearly from Fig. 5(a). The following proposition will be instrumental in developing the inversion algorithm.

Proposition 1: Consider the nonmonotonic hysteresis model (9). Let $\kappa_{\max}$ and $\kappa_{\min}$ denote the maximum output and minimum output of the model, respectively. Then, $\kappa_{\max}$ can always be achieved by first increasing the temperature T to $T_{\max}$ and then decreasing it monotonically to some value, and $\kappa_{\min}$ can always be achieved by decreasing T to $T_{\min}$ and then increasing it to some value.

Proof. For any temperature T, the memory curve consisting of a single vertical segment (intersecting the line $\alpha = \beta$ at T) dominates any other memory curves at the same temperature, in the sense that the corresponding set $P_+ \triangleq \{(\beta, \alpha) : \gamma_{\beta,\alpha} = +1\}$ in the Preisach plane is maximal for the given T. Consequently, the corresponding output κ_P of the Preisach operator (with nonnegative density function) is largest under the dominant memory curve. See Fig. 11 for illustration, and compare the two memory curves ψ' (dominant) and $\psi^{(k)}$ for the same temperature $T^{(k)}$.

The contribution κ_E depends only on the current temperature (no memory). Therefore, for a given temperature T, the maximum curvature output κ can always be achieved with an input sequence that results in a dominant memory curve at T. Such a dominant memory curve is created by decreasing the temperature from $T_{\max}$ to T. The other case follows from a similar argument. □

The curvature output κ at $T_{\max}$ and $T_{\min}$ is denoted as κ_+ and κ_-, respectively. Due to the positive/negative saturation, κ_+ and κ_- are uniquely defined and independent of the initial condition of the operator Ω. The following assumption is made:

$$\text{Assumption1:} \quad \kappa_{\min} < \kappa_- \leq \kappa_+ \leq \kappa_{\max}. \tag{18}$$

The assumption is expected to hold for all VO_2-based microbending actuators. In particular, for the sample used in this paper, $\kappa_{\max} = 1836\ \mathrm{m}^{-1}, \kappa_+ = 1828\ \mathrm{m}^{-1}, \kappa_- = -20\ \mathrm{m}^{-1}$, and $\kappa_{\min} = -75\ \mathrm{m}^{-1}$.

A. Inversion Algorithm

For brevity purposes, only the case $\bar{\kappa} > \kappa^{(0)}$ is discussed; the case $\bar{\kappa} < \kappa^{(0)}$ is treated in a symmetric manner. If $\bar{\kappa} > \kappa^{(0)}$, the discussion is divided into two subcases: 1) $\bar{\kappa} \leq k_+$ and 2) $\kappa_+ < \bar{\kappa} \leq \kappa_{\max}$. For the first case, an iterative procedure modified from [15] is detailed; for the second case, the required input will be a two-step sequence and the procedure is outlined. Specifically

If $\bar{\kappa} \leq \kappa_+$

1) Step 1: $k := 0$.
2) Step 2:
   a) Determine $d_1^{(k)} > 0$ such that $T^{(k)} + d_1^{(k)}$ equals the next discrete input level.
   b) Determine the minimum $d_2^{(k)} > 0$ such that $T^{(k)} + d_2^{(k)}$ would erase the next corner of the memory curve $\psi^{(k)}$, which is generated under the iterative input sequence $\{T^{(0)}, T^{(1)}, \ldots, T^{(k)}\}$.
   c) Evaluate the coefficients $a_1^{(k)}, a_2^{(k)}, c_1^{(k)}, c_2$ for (13) and (16), whose values are determined by $\psi^{(k)}$ and $T^{(k)}$ and vary from iteration to iteration. Solve the equation

$$\bar{\kappa} - \Omega[T^{(k)}, \psi^{(k)}] = (a_2^{(k)} - c_2)d^2 + (a_1^{(k)} - c_1^{(k)})d \tag{19}$$

   for d. If (19) has two positive solutions, let $d_0(k)$ be the smaller solution; if (19) has one positive solution, let $d_0^{(k)}$ equal that solution; and if (19) has no positive solutions, let $d_0^{(k)} = 1000$ (a number larger than $(T_{\max} - T_{\min})/M$ but otherwise arbitrary). This scheme ensures the uniqueness of the solution.
   d) Let $d^{(k)} =: \min\{d_0^{(k)}, d_1^{(k)}, d_2^{(k)}\}, T^{(k+1)} = T^{(k)} + d^{(k)}, \kappa^{(k+1)} = \Omega[T^{(k+1)}; \psi^{(k)}]$.
   e) If $d^{(k)} = d_0^{(k)}$, go to Step 3; otherwise, let $k := k + 1$ and go back to Step 2.
3) Step 3: $\bar{T} := T^{(k+1)}$ and stop.

If $\kappa_+ < \bar{\kappa} \leq \kappa_{\max}$: Inversion can be realized by first applying the temperature $T_{\max}$ to saturate the Preisach operator, and then decreasing input iteratively following a similar scheme.

Note that the inversion algorithm requires knowing the current initial memory curve $\psi^{(0)}$. As for the inversion of a Preisach operator [21], this requirement is typically satisfied by setting the initial memory curve at time $n = 0$ to a (known) configuration that corresponds to positive or negative saturation of the Preisach operator Γ, by applying $T_{\max}$ or $T_{\min}$, respectively. The memory curve at any future time $n > 0$ can then be inferred based on the curve at $n - 1$ and the sequence of input values applied after time $n - 1$. The following proposition summarizes the properties of the proposed inversion algorithm.

Proposition 2: The proposed inversion algorithm produces the input $\bar{T}$ satisfying $\Omega[\bar{T}; \psi^{(0)}] = \bar{\kappa}$ in no more than $n_c(\psi^{(0)}) + M$ iterations, where $n_c(\psi^{(0)})$ denotes the number of corners in $\psi^{(0)}$, and M is the discretization level. Furthermore, $\bar{T}$ has no more than two elements.

Proof. The case where $\bar{\kappa} > \kappa^{(0)}$ is proved in detail. First, consider the case $\bar{\kappa} < \kappa_+$. Since the operator Ω is continuous (i.e., its output changes continuously with the input), there must exist $\bar{T} \in [T^{(0)}, T_{\max}]$ such that $\Omega[\bar{T}; \psi^{(0)}] = \bar{\kappa}$. The inversion algorithm then searches for the exact solution in contiguous segments within $[T^{(0)}, T_{\max}]$, where the segments are defined by the discrete input levels and the memory curve $\psi^{(0)}$. The number of such segments is no greater than $n_c(\psi^{(0)}) + M$, which provides the upper bound for the iteration steps. The case of $\kappa_+ < \bar{\kappa} \leq \kappa_{\max}$ can be proved following similar and simpler arguments. Applying first $T_{\max}$ erases all the memory curve corners, so it is only needed to search within segments defined by the discrete input levels. The maximum iteration steps will be M in this case. The last statement of the proposition is evident from the description of the algorithm. □

From Proposition 2, the efficiency of the proposed inverse compensation algorithm in this paper is comparable to that of the inversion algorithm for a Preisach operator [15].

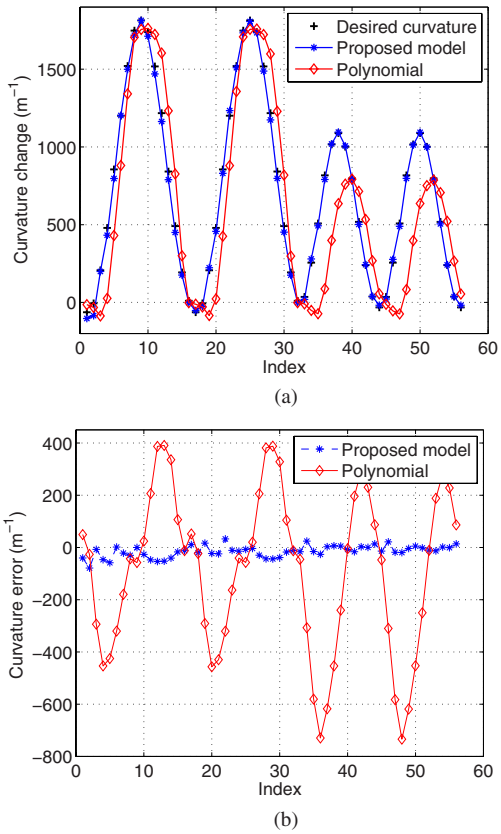

Fig. 12. (a) Open-loop inverse control performance for the proposed model and the polynomial model. (b) Inverse compensation errors.

B. Experimental Validation

The performance of the proposed inversion algorithm has been examined in open-loop curvature tracking experiments. For comparison, the single-valued polynomial model has also been inverted through a lookup table. The desired curvature is chosen to be from -63 to 1814 m^{-1} to test the effectiveness of the inverse compensation algorithm for a wide curvature range.

Fig. 12(a) shows the curvature outputs obtained under the two inversion schemes and Fig. 12(b) shows the corresponding inversion errors. The inversion of the proposed model is proven to be effective, with the largest curvature error of 78 m^{-1}, which is only 4.1% of the whole curvature range. In comparison, the inversion of the nonhysteretic polynomial model produces a maximum error of 734.2 m^{-1}. The root-mean-square error (RMSE) value is also calculated to quantify the tracking error. The RMSE of the proposed inversion is only 26.7 m^{-1}, compared to 320.6 m^{-1} for the polynomial case. The last observation from Fig. 12(b) is that when the magnitude of the desired curvature changes, the proposed inversion scheme can still maintain a small curvature error, while the inversion based on the polynomial model produces a large error.

VI. Conclusion and Future Work

In this paper, a novel model was proposed for the nonmonotonic hysteretic relationship between the bending curvature and the temperature input for VO_2-coated microcantilevers. The model comprises a classical Preisach hysteresis operator and a quadratic operator that account for the phase transition-induced bending and the differential thermal expansion-induced bending, respectively. While the Preisach operator is phenomenological in nature, the overall model was motivated by the actuation physics of the actuator. Experimental results confirmed that the model captures the nonmonotonic hysteresis in the bending actuator with relatively small errors compared to the curvature range. Furthermore, an inverse compensation algorithm was presented for the proposed model, and its effectiveness was shown experimentally.

The hysteresis model considered in this paper is quasi-static and rate-independent, since it describes the bending behavior at the steady state under a given temperature. In future work, the model will be extended by incorporating both the thermal dynamics and mechanical dynamics of the beam. Closed-loop control of the actuator will also be investigated by combining feedback with the proposed inversion scheme.

Acknowledgment

The authors would like to thank Prof. T. Hogan at Michigan State University for facilitating the pulsed-laser deposition system used for the VO_2 thin films used in this study. The SEM images were taken at the Composite Materials and Structures Center at Michigan State University.

References

[1] M. Marezio, D. B. McWhan, J. P. Remeika, and P. D. Dernier, "Structural aspects of the metal-insulator transitions in Cr-doped VO_2," *Phys. Rev. B*, vol. 5, pp. 2541–2551, 1972.

[2] E. Merced, R. Cabrera, H. Coy, F. E. Fernández, and N. Sepúlveda, "Frequency tuning of VO_2-coated buckled microbridges," *J. Microelectromech. Syst.*, vol. 20, no. 3, pp. 558–560, 2011.

[3] A. Rúa, F. E. Fernández, and N. Sepúlveda, "Bending in VO_2-coated microcantilevers suitable for thermally activated actuators," *J. Appl. Phys.*, vol. 107, no. 7, pp. 074506-1–074506-4, 2010.

[4] R. Cabrera, E. Merced, N. Sepúlveda, and F. E. Fernández, "Dynamics of photothermally driven VO_2-coated microcantilevers," *J. Appl. Phys.*, vol. 110, no. 9, pp. 094510-1–094510-8, 2011.

[5] E. Merced, N. Dávila, D. Torres, R. Cabrera, F. E. Fernández, and N. Sepúlveda, "Photothermal actuation of VO_2: Cr-coated microcantilevers in air and aquous media," *Smart Mater. Struct.*, vol. 21, pp. 105009-1–105009-9, 2012.

[6] R. Cabrera, E. Merced, N. Dávila, F. E. Fernández, and N. Sepúlveda, "A multiple-state micro-mechanical programmable memory," *Microelectron. Eng.*, vol. 88, no. 11, pp. 3231–3234, 2011.

[7] G. Song, J. Q. Zhao, X. Q. Zhou, and J. A. de Abreu Garcia, "Tracking control of a piezoceramic actuator with hysteresis compensation using inverse Preisach model," *IEEE/ASME Trans. Mechatronics*, vol. 10, no. 2, pp. 198–209, Apr. 2005.

[8] S. Bashash and N. Jalili, "Robust adaptive control of coupled parallel piezo-flexural nanopositioning stages," *IEEE/ASME Trans. Mechatronics*, vol. 14, no. 1, pp. 11–20, Feb. 2009.

[9] Y. L. Zhang, M. L. Han, M. Y. Yu, C. Y. Shee, and W. T. Ang, "Automatic hysteresis modeling of piezoelectric micromanipulator in vision-guided micromanipulation systems," *IEEE/ASME Trans. Mechatronics*, vol. 17, no. 3, pp. 547–553, Jun. 2012.

[10] M. Al Janaideh, S. Rakheja, and C.-Y. Su, "An analytical generalized Prandtl-Ishlinskii model inversion for hysteresis compensation in micropositioning control," *IEEE/ASME Trans. Mechatronics*, vol. 16, no. 4, pp. 734–744, Aug. 2011.

[11] Y. Qin, Y. Tian, and D. Zhang, "A novel direct inverse modeling approach for hysteresis compensation of piezoelectric actuator in feedforward applications," *IEEE/ASME Trans. Mechatronics*, vol. 18, no. 3, pp. 981–989, Jun. 2013.

[12] Y. Cao, C. X B, and J. Y. Peng, "An inversion-based model predictive control with an integral-of-error state variable for piezoelectric actuators," *IEEE/ASME Trans. Mechatronics*, vol. 18, no. 3, pp. 895–904, Jun. 2013.
[13] K. K. Leang, Q. Zou, and S. Devasia, "Feedforward control of piezoactuators in atomic force microscope systems," *IEEE Control Syst. Mag.*, vol. 29, no. 1, pp. 70–82, Feb. 2009.
[14] R. B. Gorbet, K. A. Morris, and D. Wang, "Passivity-based stability and control of hysteresis in smart actuators," *IEEE Trans. Control Syst. Technol.*, vol. 9, no. 1, pp. 5–16, Jan. 2001.
[15] X. Tan and J. S. Baras, "Modeling and control of hysteresis in magnetostrictive actuators," *Automatica*, vol. 40, no. 9, pp. 1469–1480, 2004.
[16] B. Drincic, X. Tan, and D. S. Bernstein, "Why are some hysteresis loops shaped like a butterfly?" *Automatica*, vol. 47, no. 12, pp. 2658–2664, 2011.
[17] X. Tan and J. S. Baras, "Adaptive identification and control of hysteresis in smart materials," *IEEE Trans. Autom. Control*, vol. 50, no. 6, pp. 827–839, Jun. 2005.
[18] D. Kucharczyk and T. Niklewski, "Accurate X-ray determination of the lattice parameters and the thermal expansion coefficients of VO_2 near the transition temperature," *J. Appl. Cryst.*, vol. 12, no. 4, pp. 370–373, 1979.
[19] Y. Okada and Y. Tokumaru, "Precise determination of lattice-parameter and thermal-expansion coefficient of silicon between 300K and 1500K," *J. Appl. Phys.*, vol. 56, no. 2, pp. 314–320, 1984.
[20] I. Mayergoyz, *Mathematical Models of Hysteresis*. New York, NY, USA: Springer-Verlag, 1991.
[21] R. V. Iyer and X. Tan, "Control of hysteretic systems through inverse compensation: Algorithm, adaption, and embedded implementation," *IEEE Control Syst. Mag.*, vol. 29, no. 1, pp. 83–99, Feb. 2009.
[22] S. Timoshenko, "Analysis of bi-metal thermostats," *J. Opt. Soc. Amer. A.*, vol. 11, no. 3, pp. 233–255, 1925.
[23] J. Nag, R. F. Haglund Jr., E. A. Payzant, and K. L. More, "Non-congruence of thermally driven structural and electronic transitions in VO_2," *J. Appl. Phys.*, vol. 112, no. 10, 2012.
[24] Z. Chen, X. Tan, and M. Shahinpoor, "Quasi-static positioning of ionic polymer-metal composite (IPMC) actuators," in *Proc. IEEE/ASME Int. Conf. Adv. Intell. Mechtronics*, 2005, pp. 60–65.
[25] D. Croft, G. Shed, and S. Devasia, "Creep, hysteresis, and vibration compensation for piezoactuators: Atomic force microscopy application," *Trans. ASME, J. Dyn. Syst., Meas. Control*, vol. 123, no. 1, pp. 35–43, 2001.
[26] S. Devasia, E. Eleftheriou, and S. O. R. Moheimani, "A survey of control issues in nanopositioning," *IEEE Trans. Control Syst. Technol.*, vol. 15, no. 5, pp. 802–823, Sep. 2007.
[27] Y. Wu and Q. Zou, "Iterative control approach to compensate for both the hysteresis and the dynamics effects of piezo actuators," *IEEE Trans. Control Syst. Technol.*, vol. 15, no. 5, pp. 936–944, Sep. 2007.

Jun Zhang (S'12) received the B.S. degree in automation from the University of Science and Technology of China, Hefei, China, in 2011. He is currently working toward the Ph.D. degree in the Department of Electrical and Computer Engineering, Michigan State University, East Lansing, USA.

His research interests include modeling and control of smart materials.

Mr. Zhang received the Student Best Paper Competition Award at the ASME 2012 Conference on Smart Materials, Adaptive Structures and Intelligent Systems.

Emmanuelle Merced received the B.Sc. and M.Sc. degrees in electrical engineering from the University of Puerto Rico, Mayagüez, Puerto Rico, in 2009 and 2011, respectively. He is currently working toward the Ph.D. degree in the Department of Electrical and Computer Engineering, Michigan State University, East Lansing, MI, USA.

His research interests include design, fabrication, and implementation of microelectromechanical actuators, smart materials-based microtransducers, control systems of hysteretic systems, and tunable microresonators.

Mr. Merced was awarded a National Science Foundation Graduate Research Fellowship in 2011.

Nelson Sepúlveda (S'05–M'06–SM'11) received the B.S. degree in electrical and computer engineering from the University of Puerto Rico, Mayagüez, Puerto Rico, in 2001, and the M.S. and Ph.D. degrees in electrical and computer engineering from Michigan State University (MSU), East Lansing, MI, USA, in 2001 and 2005, respectively. During the last year of graduate school, he attended the Sandia National Laboratories as part of a fellowship from the Microsystems and Engineering Sciences Applications program.

In January 2006, he joined the faculty of the Department of Electrical and Computer Engineering, University of Puerto Rico. He has been a Visiting Faculty Researcher at the Air Force Research Laboratories (2006 and 2007), National Nanotechnology Infrastructure Network (2008), and the Cornell Center for Materials Research (2009), the last two being the National Science Foundation (NSF) funded centers at Cornell University, Ithaca, NY, USA. In Fall 2011, he joined the faculty of the Department of Electrical and Computer Engineering, MSU, where he is currently an Assistant Professor. His current research interests include smart materials and the integration of such in microelectromechanical systems, with particular emphasis on vanadium dioxide (VO_2) thin films and the use of the structural phase transition for the development of smart microactuators.

Dr. Nelson received an NSF CAREER Award in 2010.

Xiaobo Tan (S'97–M'02–SM'11) received the B.Eng. and M.Eng. degrees in automatic control from Tsinghua University, Beijing, China, in 1995 and 1998, respectively, and the Ph.D. degree in electrical and computer engineering from the University of Maryland, College Park, MD, USA, in 2002.

From September 2002 to July 2004, he was a Research Associate with the Institute for Systems Research, University of Maryland. He joined the faculty of the Department of Electrical and Computer Engineering, Michigan State University (MSU), East Lansing, MI, USA, in 2004, where he is currently an Associate Professor. His current research interests include electroactive polymer sensors and actuators, modeling and control of smart materials, biomimetic robotic fish, mobile sensing in aquatic environments, and collaborative control of autonomous systems.

Dr. Tan is an Associate Editor of *Automatica* and a Technical Editor of the IEEE/ASME TRANSACTIONS ON MECHATRONICS. He served as the Program Chair for the 15th International Conference on Advanced Robotics in 2011. He was a Guest Editor of the *IEEE Control Systems Magazine* for its February 2009 issue's Special Section on Modeling and Control of Hysteresis. He received a National Science Foundation CAREER Award in 2006, the 2008 American Society of Mechanical Engineers Dynamic Systems and Control Division Best Mechatronics Paper Award (with Yang Fang) in 2009, and the Teacher-Scholar Award from MSU in 2010.